Supporting information for

Precise fibrin decomposition and tumor mechanics modulation with hydroxyethyl starch-based smart nanomedicine for enhanced antitumor efficacy

Jitang Chen[a], Zhijie Zhang[a], Yining Li[a], Haowen Zeng[a], Zheng Li[a], Chong Wang[a], Chen Xu[a], Qingyuan Deng[a], Qiang Wang[a], Xiangliang Yang[a,b,c,d,e], Zifu Li[a,b,c,d,f,*]

[a] National Engineering Research Center for Nanomedicine, College of Life Science and Technology, Huazhong University of Science and Technology, Wuhan, 430074, P. R. China

[b] Key Laboratory of Molecular Biophysics of Ministry of Education, College of Life Science and Technology, Huazhong University of Science and Technology, Wuhan, 430074, P. R. China

[c] Hubei Key Laboratory of Bioinorganic Chemistry and Materia Medical, Huazhong University of Science and Technology, Wuhan, 430074, P. R. China

[d] Hubei Engineering Research Center for Biomaterials and Medical Protective Materials, Huazhong University of Science and Technology, Wuhan, 430074, P. R. China

[e] GBA Research Innovation Institute for Nanotechnology, Guangdong, 510530, P. R. China

[f] Wuhan Institute of Biotechnology, High Tech Road 666, East Lake high tech Zone, Wuhan, 430040, P. R. China

* Correspondence and requests for materials should be addressed to ZFL (email: zifuli@hust.edu.cn).

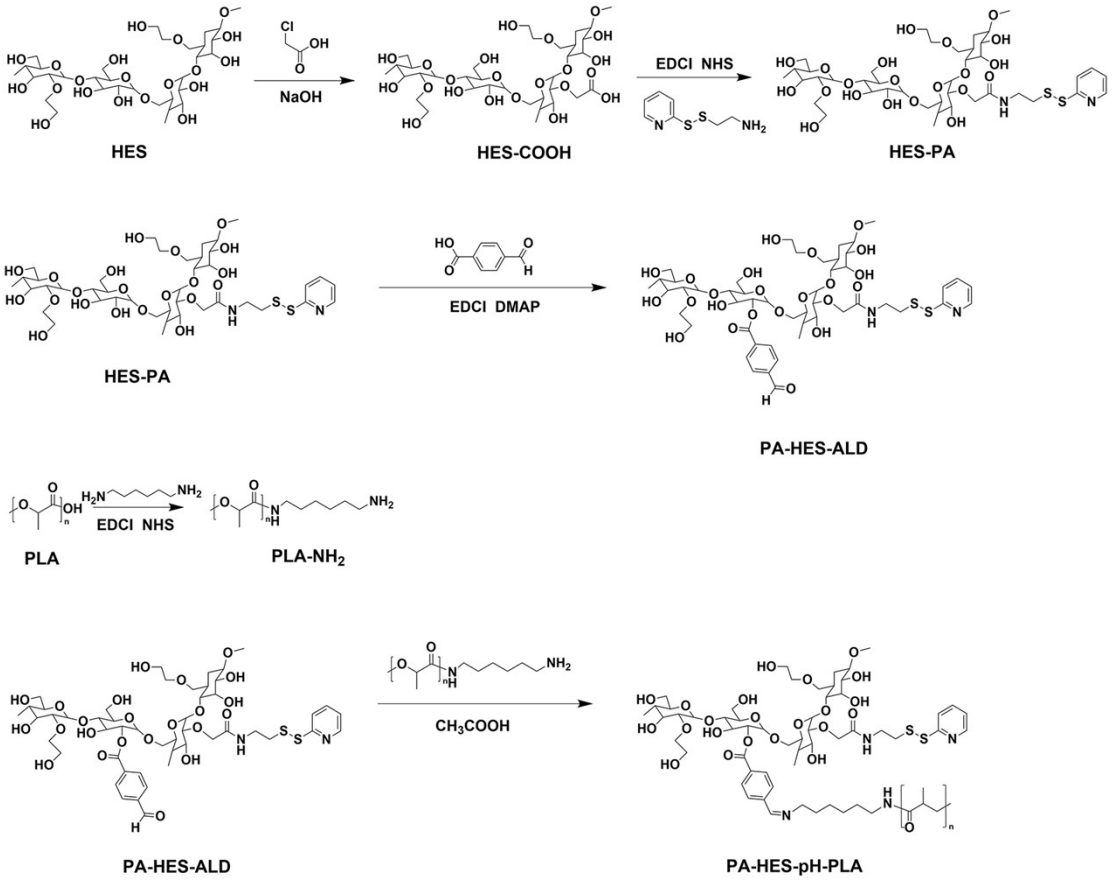

Fig. S1 Synthetic steps of PA-HES-pH-PLA. PA and 4-carboxy-benzaldehyde can randomly react with hydroxyl groups in HES molecules, and HES-PA, PA-HES-ALD and PA-HES-pH-PLA drawn here are structural schematic diagrams.

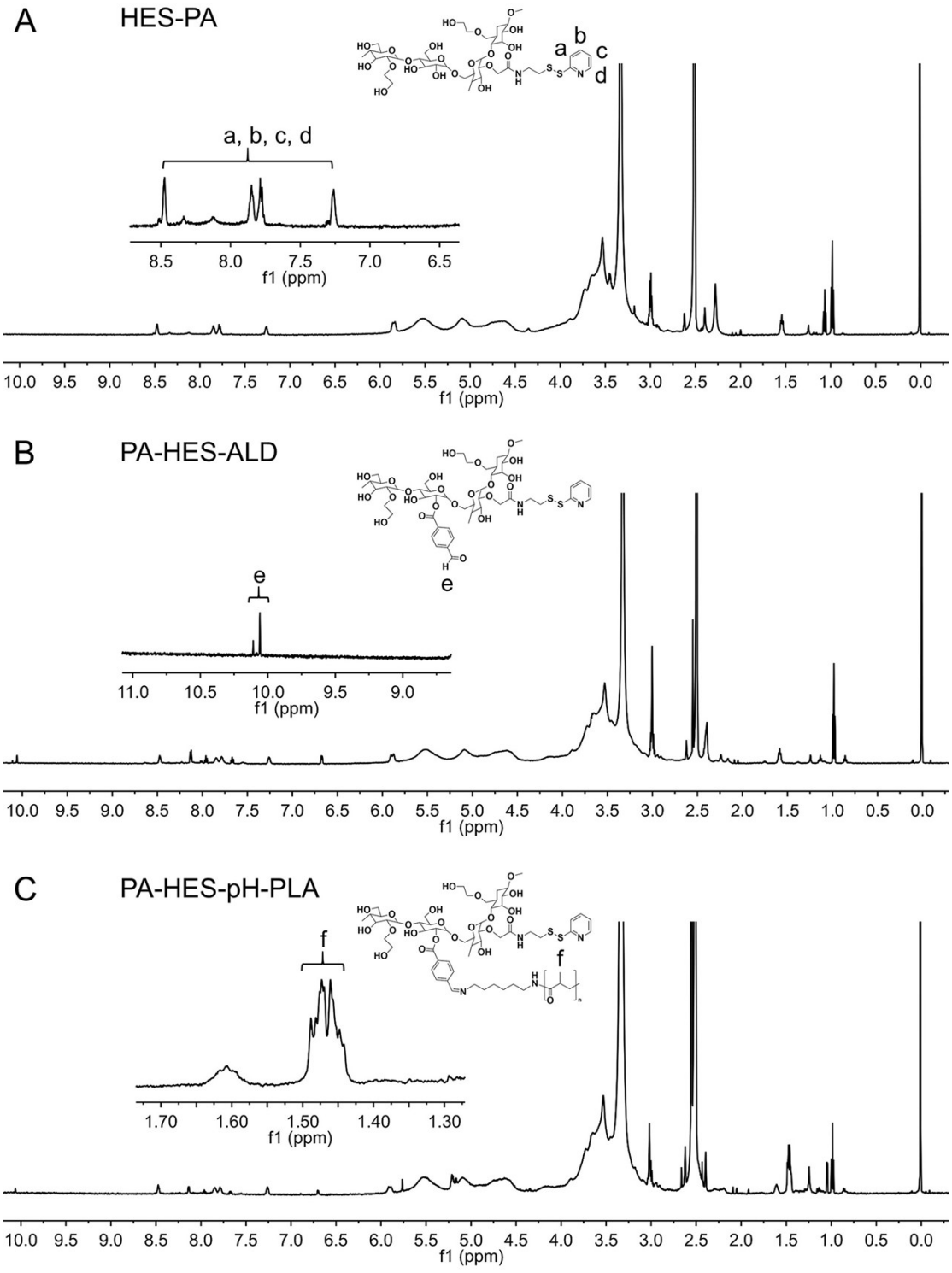

Fig. S2 ^{1}H NMR spectra of (A) HES-PA, (B) PA-HES-ALD, and (C) PA-HES-pH-PLA.

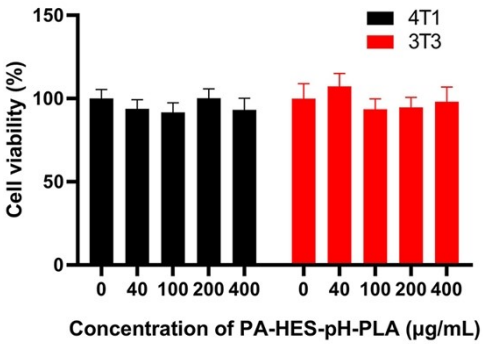

Fig. S3 Cytotoxicity of PA-HES-pH-PLA on 4T1 cells and 3T3 fibroblasts (n = 5-6). Data represent the mean ± SEM.

Table S1 Drug loading contents and drug loading efficiencies of nanoparticles. Data represent the mean ± SEM (n = 3).

Group	Drug loading content (%)		Drug loading efficiency (%)	
	DOX	tPA	DOX	tPA
DOX@CREKA/tPA-HP	4.18 ± 0.21	5.17 ± 0.12	48.94 ± 2.15	75.65 ± 2.18
DOX@HP	4.98 ± 0.12	-	52.41 ± 1.28	-
DOX@tPA-HP	4.43 ± 0.14	5.31 ± 0.31	49.12 ± 1.74	84.14 ± 5.31

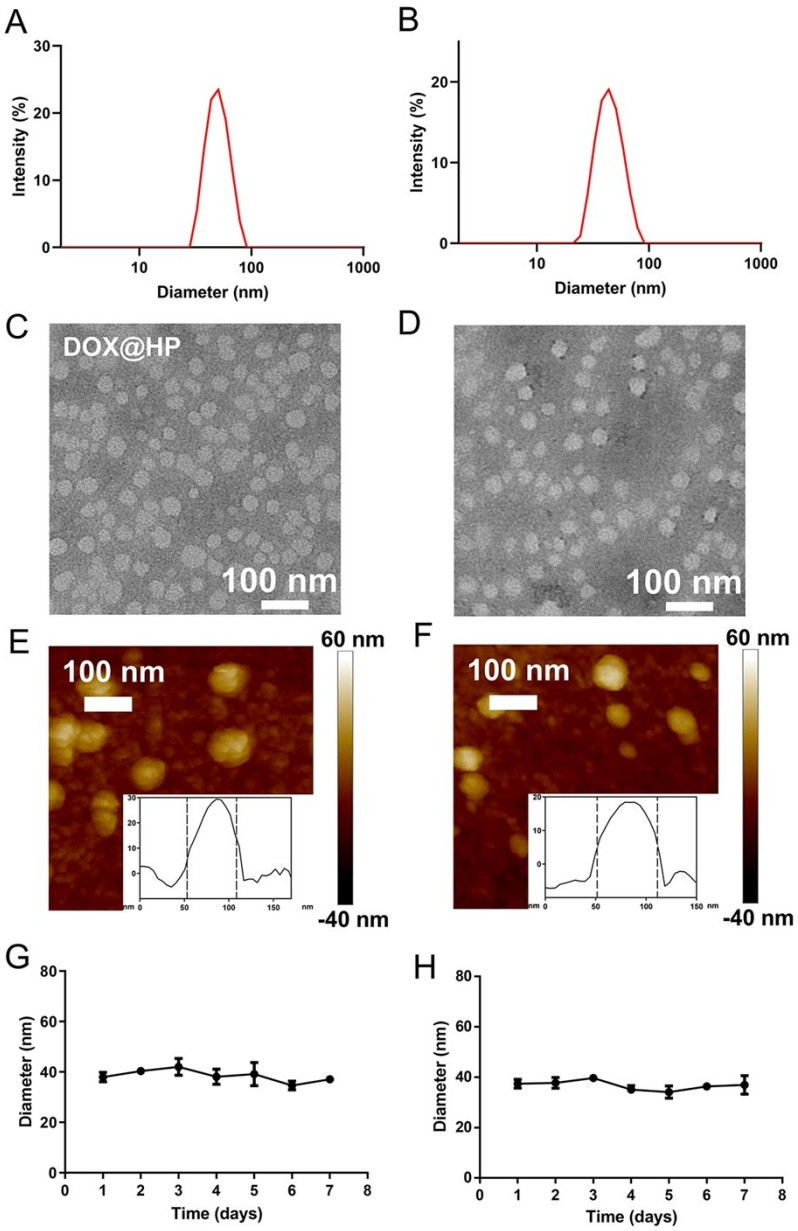

Fig. S4 Characterization of DOX@HP and DOX@tPA-HP. Hydrodynamic diameter distribution of (A) DOX@HP and (B) DOX@tPA-HP. TEM images of (C) DOX@HP and (D) DOX@tPA-HP. The scale bar is 100 nm. AFM images of (E) DOX@HP and (F) DOX@tPA-HP. The scale bar is 100 nm. Stability of (G) DOX@HP and (H) DOX@tPA-HP in PBS (n = 3). Data represent the mean ± SEM.

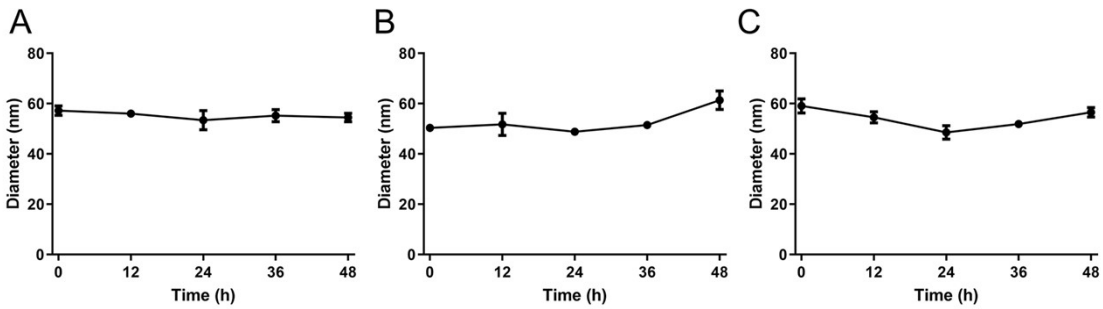

Fig. S5 Stability of (A) DOX@CREKA/tPA-HP, (B) DOX@HP and (C) DOX@tPA-HP in PBS buffer containing 10% FBS (n = 3).

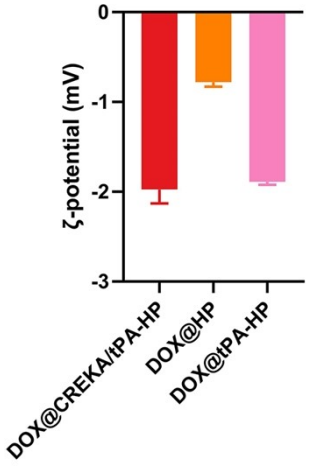

Fig. S6 ζ-potentials of DOX@CREKA/tPA-HP, DOX@HP and DOX@tPA-HP (n = 3).

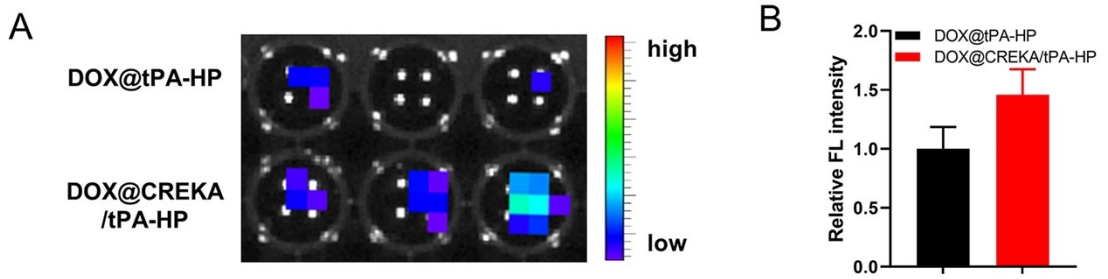

Fig. S7 (A) Fluorescence intensity and (B) quantification results of residual DOX@tPA-HP and DOX@CREKA/tPA-HP in fibrin gel after PBS washing for 3 times (n = 3). Data represent the mean ± SEM.

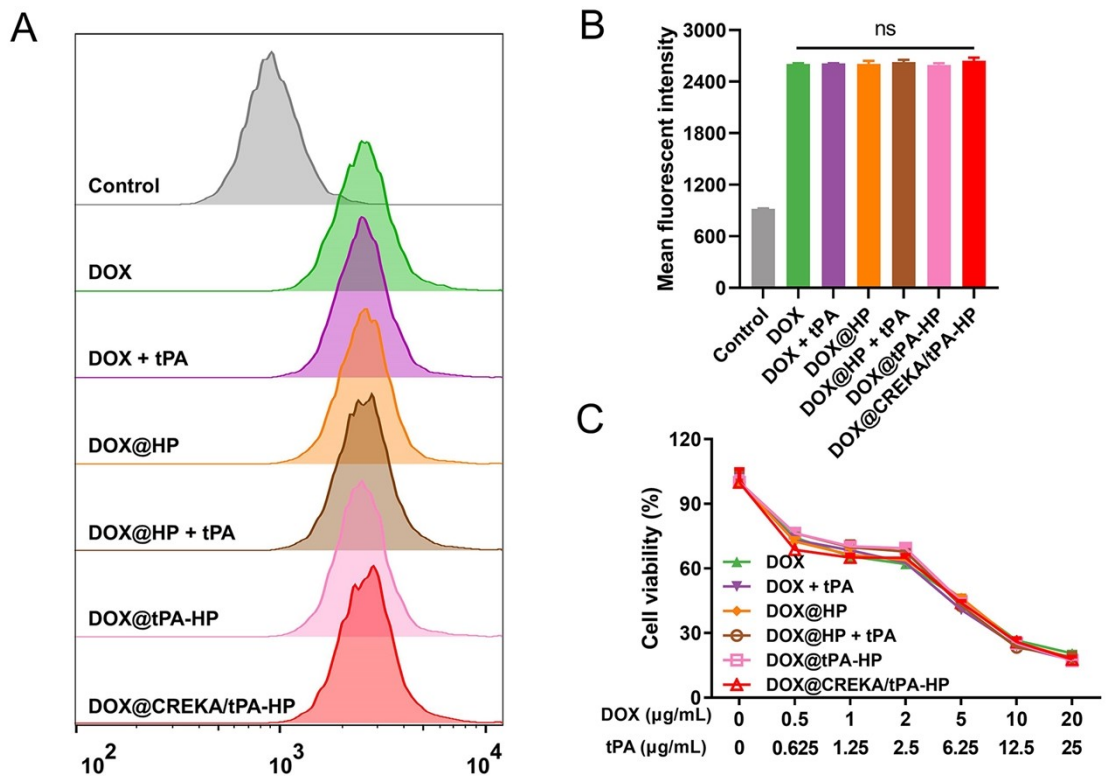

Fig. S8 (A) Cellular uptake of DOX in 4T1 cells measured by flow cytometry and (B) its quantification (n = 4). (C) Cytotoxicity of DOX@CREKA/tPA-HP after 4T1 cells have been incubated for 24 h (n = 6). ns stands for not significant. Data represent the mean ± SEM.

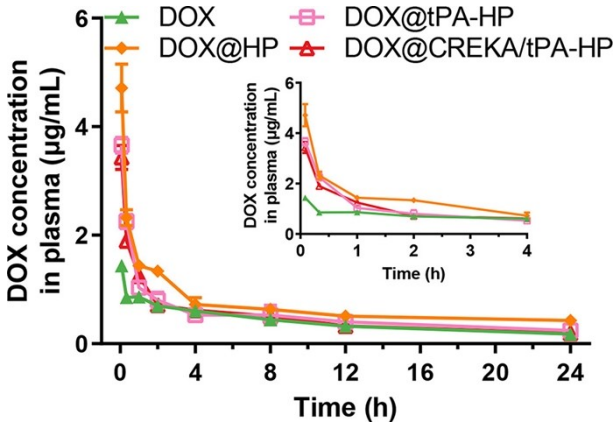

Fig. S9 Drug plasma concentration-time profiles of DOX, DOX@HP, DOX@tPA-HP and DOX@CREKA/tPA-HP after intravenous administration in mice. Data represent the mean ± SEM (n = 3).

Table S2 Pharmacokinetic parameters of DOX, DOX@HP, DOX@tPA-HP and DOX@CREKA/tPA-HP after intravenous administration in mice. Data represent the mean ± SEM (n = 3).

Parameters	DOX	DOX@HP	DOX@tPA-HP	DOX@CREKA /tPA-HP
Dosage (mg DOX·kg^{-1})	4	4	4	4
C_{max} (μg·mL^{-1})	1.44 ± 0.15	4.71 ± 0.63^{a}	3.66 ± 0.21^{c}	3.43 ± 0.32^{b}
$t_{1/2}$ (h)	10.07 ± 3.45	13.01 ± 6.48	14.74 ± 5.34	13.24 ± 1.93
CL (L·h^{-1}·kg^{-1})	0.35 ± 0.11	0.19 ± 0.03	0.26 ± 0.12	0.27 ± 0.02
AUC $_{(0\rightarrow t)}$ (mg·h·L^{-1})	9.68 ± 1.82	16.58 ± 0.68^{a}	12.25 ± 2.92	11.36 ± 1.04

The pharmacokinetic parameters were calculated according to non-compartment model. C_{max}, maximum plasma concentration. $t_{1/2}$, elimination half-life time. CL, clearance rate. AUC, area under curve. a represents $p < 0.05$, b represents $p < 0.01$, and c represents $p < 0.001$, relative to DOX group.

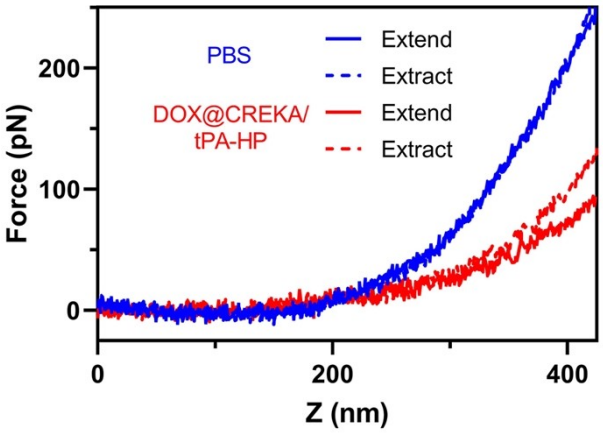

Fig. S10 Typical force curves for extend and retract processes obtained on tumor slices.

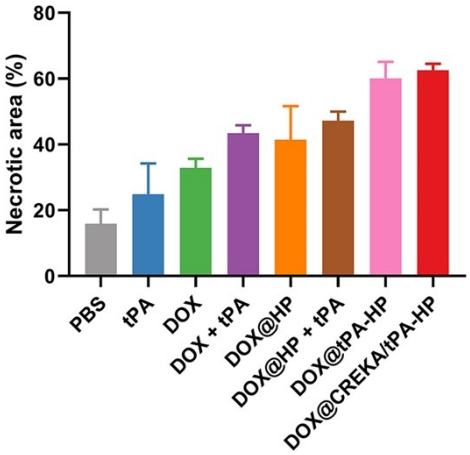

Fig. S11 Necrotic area of tumor sections (n = 3). Data represent the mean ± SEM.

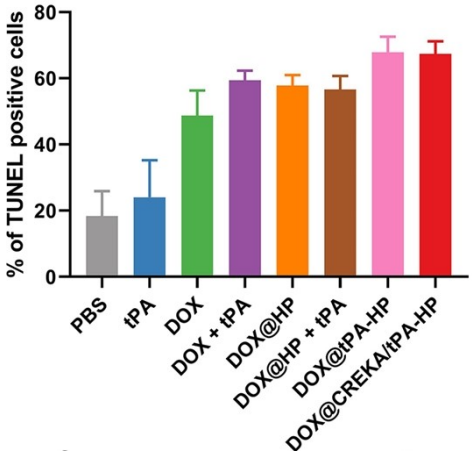

Fig. S12 Percentage of TUNEL positive cells in tumor sections (n = 3). Data represent the mean ± SEM.

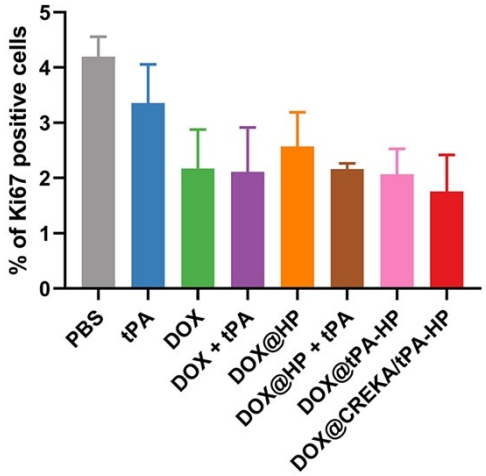

Fig. S13 Percentage of Ki67 positive cells in tumor sections (n = 3). Data represent the mean ± SEM.

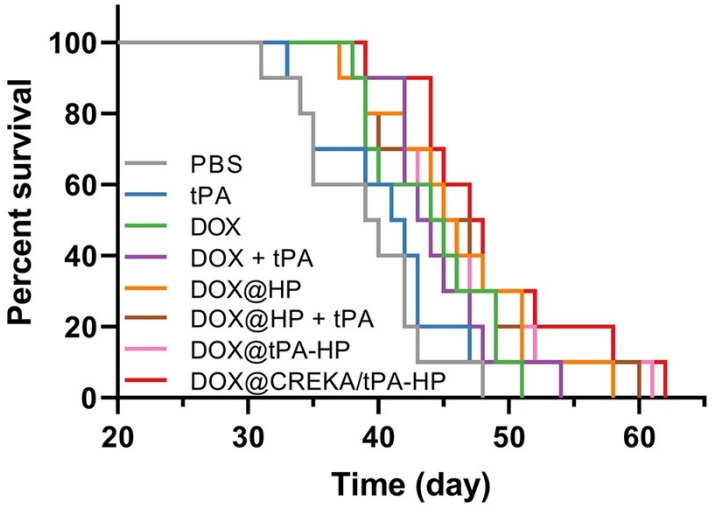

Fig. S14 Survival curves of 4T1 tumor-bearing mice with different treatments.

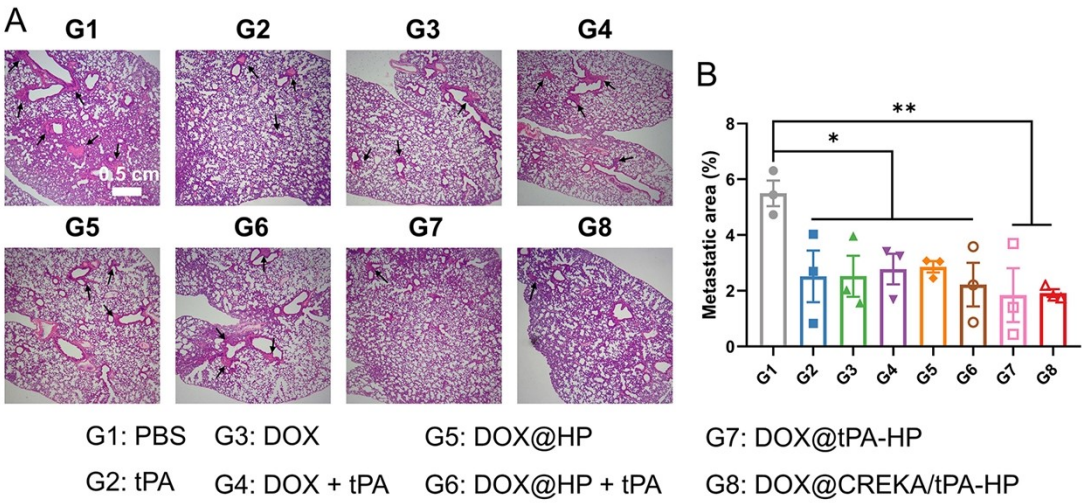

Fig. S15 (A) Images of tumor metastasis in lungs after different treatments in 4T1 tumor models. Black arrows represent metastatic areas. The scale bar is 0.5 cm. (B) Percentage of metastatic area in lungs after different treatments (n = 3). *$p < 0.05$, **$p < 0.01$. Data represent the mean ± SEM.

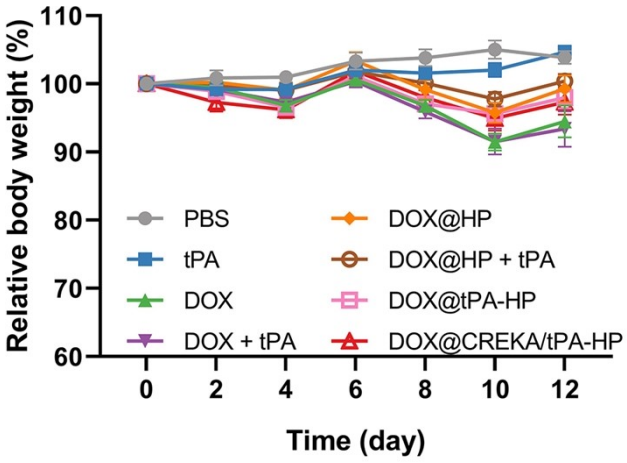

Fig. S16 Body weights of 4T1 tumor-bearing mice with different treatments (n = 6). Data represent the mean ± SEM.

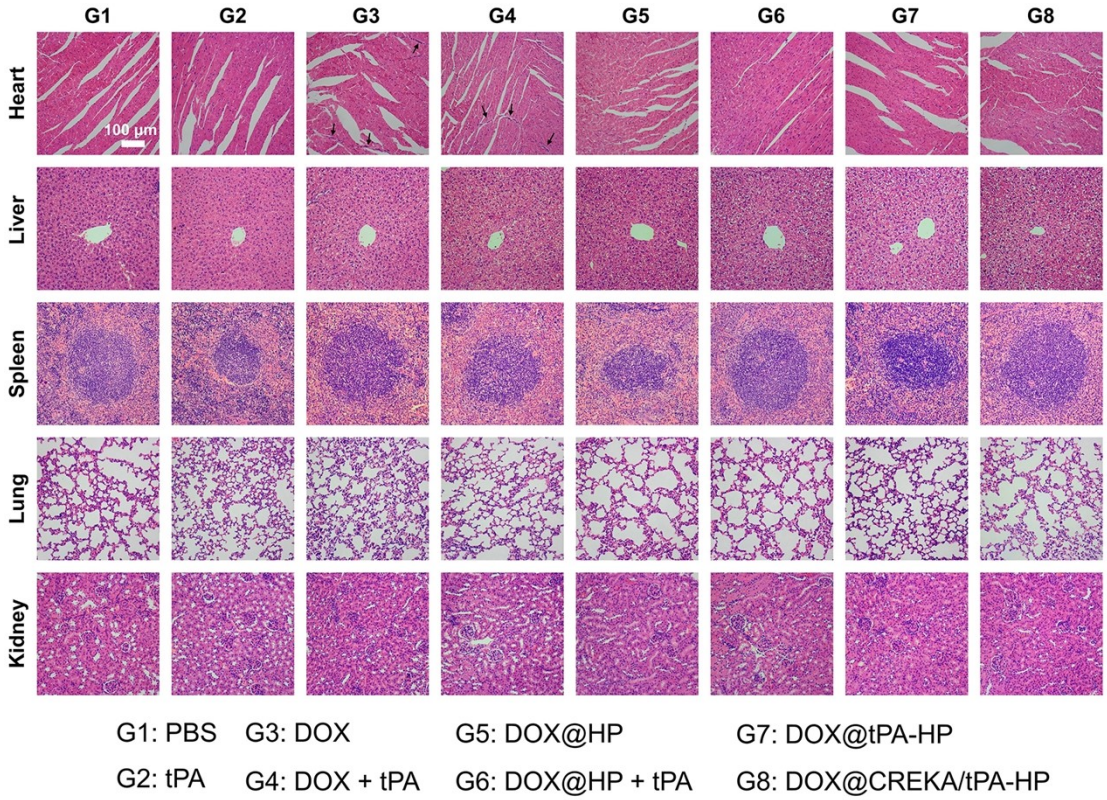

Fig. S17 H&E staining of major organs at the end of the *in vivo* antitumor experiment. Black arrows represent lesions. The scale bar is 100 μm.

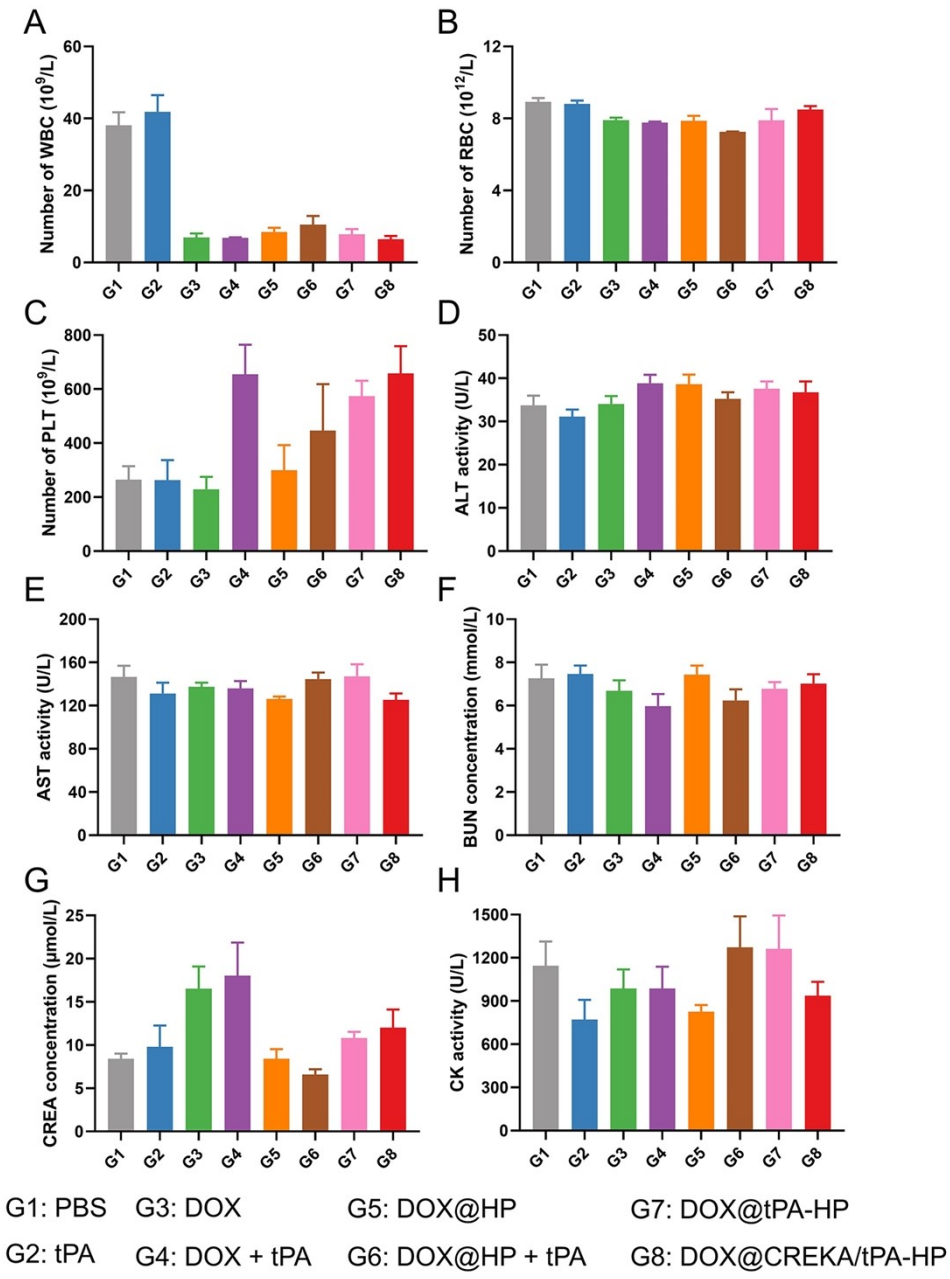

Fig. S18 Biocompatibility assay of various treatments. Numbers of (A) white blood cells (WBC), (B) red blood cells (RBC) and (C) platelets (PLT) in 4T1 tumor-bearing mice after different treatments. Serological analysis of (D) alanine aminotransferase (ALT), (E) aspartate aminotransferase (AST), (F) blood urea nitrogen (BUN), (G) creatinine (CREA) and (H) creatine kinase (CK) in 4T1 tumor-bearing mice with different treatments. Data represent the mean ± SEM (n = 5).